



**HAL**  
open science

## Pure copper components fabricated by cold spray (CS) and selective laser melting (SLM) technology

Jian Huang, Xingchen Yan, Cheng Chang, Yingchun Xie, Wenyu Ma,  
Renzhong Huang, Ruimin Zhao, Shunhua Li, Min Liu, Hanlin Liao

### ► To cite this version:

Jian Huang, Xingchen Yan, Cheng Chang, Yingchun Xie, Wenyu Ma, et al.. Pure copper components fabricated by cold spray (CS) and selective laser melting (SLM) technology. *Surface and Coatings Technology*, 2020, 395, pp.125936. 10.1016/j.surfcoat.2020.125936 . hal-02634321

**HAL Id: hal-02634321**

**<https://utt.hal.science/hal-02634321>**

Submitted on 22 Aug 2022

**HAL** is a multi-disciplinary open access archive for the deposit and dissemination of scientific research documents, whether they are published or not. The documents may come from teaching and research institutions in France or abroad, or from public or private research centers.

L'archive ouverte pluridisciplinaire **HAL**, est destinée au dépôt et à la diffusion de documents scientifiques de niveau recherche, publiés ou non, émanant des établissements d'enseignement et de recherche français ou étrangers, des laboratoires publics ou privés.



Distributed under a Creative Commons Attribution - NonCommercial 4.0 International License

# 1 Pure copper components fabricated by cold spray (CS) and 2 selective laser melting (SLM) technology

3 Jian HUANG<sup>1</sup>, Xingchen YAN<sup>1,2\*</sup>, Cheng CHANG<sup>3\*</sup>, Yingchun XIE<sup>1</sup>, Wenyu MA<sup>1</sup>, Renzhong  
4 HUANG<sup>1</sup>, Ruimin ZHAO<sup>4</sup>, Shunhua LI<sup>4</sup>, Min LIU<sup>1</sup>, Hanlin LIAO<sup>2</sup>

5 1. National Engineering Laboratory for Modern Materials Surface Engineering Technology; The  
6 Key Lab of Guangdong for Modern Surface Engineering Technology; Guangdong Institute of New  
7 Materials, Guangzhou 510651, P.R. China

8 2. ICB UMR 6303, CNRS, Univ. Bourgogne Franche-Comté, UTBM, F-90010 Belfort, France

9 3. ICD-LASMIS, UMR CNRS 6281, University of Technology of Troyes, 12 rue Marie Curie, CS  
10 42060, 10004, Troyes Cedex, France

11 4. Yunnan Yunlu Yongxin Co., Ltd, Honghe, 654300, P.R. China

## 12 Abstract:

13 To study effect of the different metal additive manufacturing techniques on  
14 microstructural evolution, phase constitution and the relationship between the  
15 microstructure and tensile behaviour of pure Cu parts, components were  
16 manufactured by selective laser melting (SLM) technology and cold spraying (CS)  
17 technology, respectively. The microstructure of Cu parts was detected using an optical  
18 microscope (OM) and scanning electron microscopy (SEM). The XRD spectrum  
19 revealed that only Cu phase is formed in the SLM Cu and CS Cu samples. The  
20 microstructure of the SLM Cu samples is constituted by the polycrystalline grains  
21 with substructures including the columnar dendrites and the equiaxed structures. As  
22 for the CS Cu samples, only the equiaxed grains were detected. In terms of the main  
23 physical properties, the averaged electrical conductivity of SLM Cu sample is 41 %  
24 IACS, while that of CS Cu sample is 73 % IACS. For the microhardness, the mean  
25 microhardness value of the CS Cu and the SLM Cu samples is  $144.2 \pm 4.3$  HV<sub>0.05</sub> and  
26  $83.6 \pm 5.2$  HV<sub>0.05</sub>, respectively. With regard to the statistic mechanical properties, the  
27 yield strength (YS) and ultimate tensile strength (UTS) of the SLM Cu part is  
28 approximately  $185.8 \pm 6.1$  MPa and  $242.2 \pm 8.2$  MPa, respectively.

29

30 **Keywords:** Selective laser melting, Pure copper, Cold spraying, Microstructure evolution,  
31 Mechanical property.

1

\*Corresponding authors.

E-mail addresses: Xingchen YAN: [yanxingchen0802@163.com](mailto:yanxingchen0802@163.com),

Cheng CHANG: [cheng.chang1993@hotmail.com](mailto:cheng.chang1993@hotmail.com).

## 32 1 Introduction

33 Different from conventional subtractive manufacturing technologies, additive  
34 manufacturing (AM) processes are a series of manufacturing methods based on a  
35 “bottom-up” processing concept [1,2]. In a narrow sense, AM indicates layer-wise  
36 creating and forming of powders/wires to almost arbitrary geometry forms, usually  
37 through melting and fusing them via a computer controlled high-power energy source,  
38 e.g. laser, electron beam, and/or arc [3,4]. With regard to metal-based materials, the  
39 powders/wires are melted by a high-energy heat source and then rapidly solidified to  
40 generate unique microstructures resulting from the non-equilibrium cooling  
41 conditions. Owing to this twinkling feature, parts produced using metal AM can reach  
42 or exceed the mechanical properties of the wrought counterparts. Hence,  
43 complex-shaped components of Ti-, Fe-, Ni-based alloys, or metal matrix composites  
44 [5,6] have been successfully manufactured employing the metal AM, especially  
45 utilizing selective laser melting (SLM) technology [7,8]. Yan et al. [9] reported that  
46 the isotropic Ti6Al4V octahedral lattice structures were designed and manufactured  
47 successfully using SLM technology for application as human bone substitutes. The  
48 results demonstrated that the lattice structures with biocompatible surfaces had an  
49 equivalent compressive strength (71-190 MPa) and elastic modulus (2.1-4.7 GPa) to  
50 trabecular bone. Saedi et al. [10] showed that SLM porous NiTi parts with up to 58 %  
51 porosity could be fabricated with full recovery under 100 MPa nominal stress. Yan et  
52 al. [11] produced WC particles reinforced maraging steel 300 components with good  
53 wear-resistance performance via SLM technology. However, metallic materials  
54 suitable for SLM processing have to meet three basic requirements, i.e. high laser  
55 absorption, low thermal conductivity and without low boiling point elements. These  
56 characteristics seem extremely unfriendly to low melting metal materials, such as Al-,  
57 Mg-, or Cu-based alloys. Therefore, partial/non-melting AM processes are of great  
58 need.

59 In a wide sense of the word, besides traditional AM techniques, metal AM  
60 techniques include not only a variety of atomic-scale deposition processes, e.g.  
61 chemical vapor deposition (CVD), physical vapor deposition (PVD), electro-chemical  
62 deposition and so on, but also several solid-state welding processes, e.g. friction  
63 welding, cold spray, ultrasonic welding, etc. Among these technologies, cold spray  
64 (CS) technology, an emerging solid-state connection method, has been mainly used  
65 for a preparation of metal-based specific mechanical structures or parts [12,13].  
66 Differing from the high-temperature deposition means, the formation of cold-sprayed  
67 deposits is principally determined by the huge kinetic energy generated by high-speed  
68 raw particles, not their thermal energy. During the CS manufacturing process, the

69 feedstock particles can be accelerated to a high velocity (about 300-1200 m/s) via a  
70 low-temperature (approximate 300-1000 °C) supersonic compressed gas flow (usually  
71 nitrogen or helium) [14–16]. Then, the dense deposition parts can be obtained layer  
72 by layer through the deformation-induced particle-matrix and particle-particle  
73 mechanical interlocking and/or cold welding process. Notably, due to the low  
74 temperature of the propelling inert gas beneath the melting point of the raw particles  
75 and the extremely short interaction time between these particles (in order of  
76 nanoseconds), the deposited powder particles can still remain the solid state after CS  
77 processing. As a result, some inevitable defects, such as oxidation, residual thermal  
78 stress, or phase transformation, which often occur in the high-temperature deposition  
79 approaches, can be avoid. Thanks to the nature of the CS technology, it is an  
80 indispensable way employed for a production of low melting and easily oxidizable  
81 metal-based materials. Wang et al. [17] successfully generated CS Al-Al<sub>2</sub>O<sub>3</sub> coatings  
82 on AZ91D substrate and the bond strength of the composite coatings with the  
83 substrate was better than the coatings themselves. Yin et al. [18] revealed the  
84 deposition behavior of thermally softened particles in cold spraying process by  
85 analyzing the results of the preheated Cu particles deposited onto Cu substrate. Chen  
86 et al. [19] demonstrated that the isostatic pressing (HIP) treatment could be adopted to  
87 reduce the interior defects, adjust the microstructure, and improve the mechanical  
88 properties of the CS Ti6Al4V parts. Bagherifard et al. [20] fabricated the freestanding  
89 samples of CuCr1Zr alloy with the different volume fraction of the microcrystalline  
90 (MC) and nanocrystalline (NC) powder particles. They demonstrated that cold spray  
91 deposition was found to have a high potential for fabrication of freestanding bimodal  
92 materials with heterogeneous phase structure. In addition to the unique properties that  
93 can be imparted to the surface of the parts using CS technology, this technique also  
94 exhibits great potential in metal parts manufacture and remanufacture work. Thus, it is  
95 more and more significant to evaluate the mechanical properties of solid-state metal  
96 parts prepared via CS technology.

97 Owing to the excellent thermal conductivity (391 W/ (m·°C) at 20 °C) and  
98 electrical conductivity (103.6 % IACS at 20 °C), pure Cu is one of the most widely  
99 used engineering materials [21]. These brilliant properties have stimulated the  
100 widespread applications of the pure copper in industrial production. In some industrial  
101 applications, only pure Cu coatings are needed to improve or modify the surface  
102 properties of components; while in other industrial fields, pure Cu materials are  
103 required to be fabricated into the complex-shape parts for special purpose [22–24]. To  
104 satisfy various demands of different industrial applications, related researches on the  
105 fabrication of pure Cu components using SLM and CS technology have been  
106 launched. In the research of SLM Cu, Silbernagel et al. [25] reported that the  
107 heat-treated SLM Cu parts had lower resistivity than the as-fabricated SLM Cu

108 specimens, and the lowest average resistivity was achieved using a 1000 °C heat  
 109 treatment for four hours. With regard to the CS Cu, Yin et al. [26] investigated the  
 110 microstructure and mechanical anisotropy of cold spray copper samples. The  
 111 experimental studies indicated that CS deposits exhibited anisotropy of microstructure  
 112 and mechanical properties and the anisotropic level could be affected by post heat  
 113 treatment and nozzle scanning strategy. Li et al. [27] quantitatively investigated the  
 114 effect of the Cu particle impact velocity on the corresponding microstructure and  
 115 properties. The results indicated that it is not rational to evaluate the quality of cold  
 116 sprayed metals only by the porosity. Note that these studies primarily focused on the  
 117 microstructure and physical properties of SLM or CS samples affected by the  
 118 different processing parameters or the post heat treatments. However, a  
 119 comprehensive evaluation and comparison of the main performances of SLM Cu and  
 120 CS Cu samples has never been reported. As such, the static mechanical properties and  
 121 main physical performances of Cu parts manufactured via SLM and CS technologies  
 122 are assessed and presented in this present investigation. The microstructural evolution,  
 123 phase constitution and the relationship between the microstructure and tensile  
 124 behavior are also discussed in this research to provide guidance for industrial  
 125 applications.

## 126 2 Experimental methods

### 127 2.1 Feedstock powders and manufacturing procedure

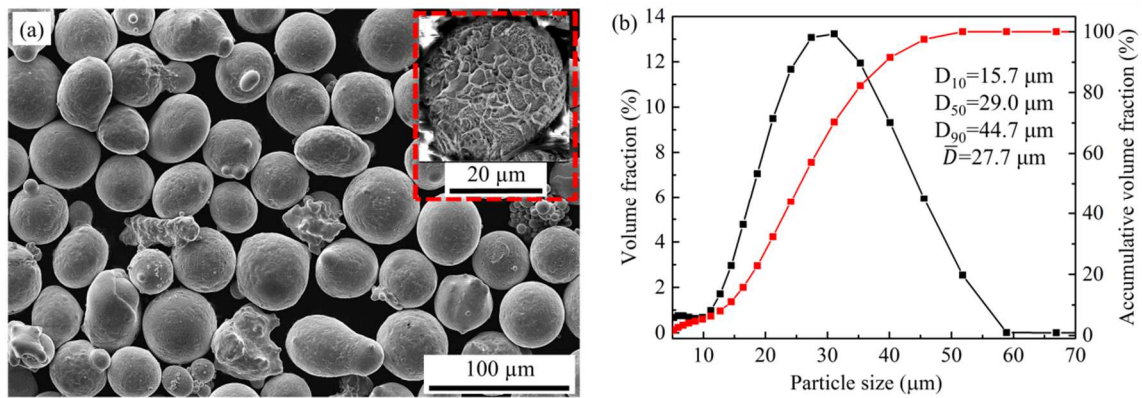
128 In this research, gas atomized commercial Cu powders (Beijing COMPO  
 129 Advanced Technology Co.) with a minimum purity of 99.9 wt. % were selected as the  
 130 raw materials. Chemical composition of this powder is presented in Table 1. The  
 131 micrograph of a pure copper powder particle is exhibited in Fig. 1a, where grain  
 132 structures are obviously noticeable. The particle size distribution ( $D_{10}=15.7 \mu\text{m}$ ,  
 133  $D_{50}=29.0 \mu\text{m}$  and  $D_{90}=44.7 \mu\text{m}$ ) was measured and displayed in Fig. 1b utilizing a  
 134 Mastersizer 2000 laser diffraction particle analyzer (Malvern Instruments Ltd., United  
 135 Kingdom). Additionally, the flowability of the pure Cu powder is 13.5 s/50 g  
 136 measured by a BT-200 Hall flowmeter (Bettersize Instruments Ltd., China), and the  
 137 tap density is  $4.9 \text{ g/cm}^3$  according to the tapping density test (BT-301, Bettersize  
 138 Instruments Ltd., China).

139 **Table 1:** Chemical composition of commercial pure Cu powder employed in this research

Elements	Ag	Fe	Ni	Pb	Zn	Sn	O	Cu
Weight (wt.) %	0.0011	0.0003	0.0012	0.0007	0.0007	0.0260	0.0423	Balance

140 The SLM Cu samples were fabricated employing an EOS M290 system (EOS

141 GmbH, Germany) equipped with a 400 W Yb-Fiber laser with a wavelength of 1064  
 142 nm and a laser spot size of 100  $\mu\text{m}$ . As presented in Fig. 2, cuboid specimens, 10 mm  
 143  $\times$  10 mm  $\times$  8 mm, and tensile samples for mechanical properties tests, were built in  
 144 the SLM working chamber. To avoid further oxidation, fabrication of the SLM Cu  
 145 parts was conducted under high-purity argon atmosphere with the oxygen content  
 146 below 0.13 %. In order to inhibit the balling phenomenon, the 316L stainless steel  
 147 substrate was preheated to a temperature of 80  $^{\circ}\text{C}$ . A zigzag scanning pattern with a  
 148 rotation angle of 67 $^{\circ}$  between neighboring layers was adopted. Table 2 lists the  
 149 detailed SLM processing parameters used in this work.



150  
 151 **Fig. 1.** (a) Macro morphology of the pure copper powder detected using SEM and the  
 152 cross-sectional microstructure of an etched single particle inserted; (b) particle size distribution of the  
 153 pure Cu powder.

154 The CS Cu specimens were deposited onto the commercial pure aluminum  
 155 substrate utilizing an in-house CS system. A 180 mm long converging-diverging De  
 156 Laval nozzle with a circular cross section is used to accelerate the gas and pure Cu  
 157 powder particles. The throat and outlet diameters are 2 mm and 6 mm, respectively.  
 158 High-purity nitrogen (minimum purity of 99 wt. %) with the inlet pressure of 4.5 MPa  
 159 and temperature of 800  $^{\circ}\text{C}$  was applied as the propulsion gas in this research and the  
 160 CS processing parameters are shown in Table 2. The powder feed rate was determined  
 161 as 200 g/min, and the nozzle movement followed the zigzag pattern. As depicted in  
 162 Fig. 2, firstly, the bulk Cu samples were fabricated via CS process. Then, CS Cu  
 163 cuboid specimens, 10 mm  $\times$  10 mm  $\times$  8 mm, and tensile specimens for mechanical  
 164 properties tests, were obtained via wire electrical discharge machining (WEDM). As  
 165 for the SLM Cu samples, the cuboid specimens and tensile specimens, as  
 166 demonstrated in Fig. 2, can be manufactured directly via SLM process. These samples  
 167 then can be obtained removed from the substrate using WEDM method. **It is clear that**  
 168 **CS Cu specimens were produced with aid of an additional procedure - cutting. Thus it**  
 169 **takes two different times. First time is for production via CS of bulk sample from**  
 170 **which metallographic and tensile specimens were cut. Hence, second time is a time**

171 for cutting.

172 **Table 2:** Fabrication parameters of the SLM and CS processes applied in this study

SLM	Laser beam diameter	Laser power	Laser beam scanning speed	Layer thickness	Hatch space	Protective atmosphere	Scanning strategy	/
	100µm	300 W	600 mm/s	30 µm	80 µm	Argon	Zigzag scanning pattern	/
CS	Working pressure	Working temperature	Standoff distance	Hatch distance	gun travel speed	Propulsion gas	Deposition strategy	Feed rate
	4.5 MPa	800 °C	30 mm	3.5 mm	50 mm/s	Nitrogen	Zigzag scanning pattern	200 g/min

173 **2.2 Material characterization**

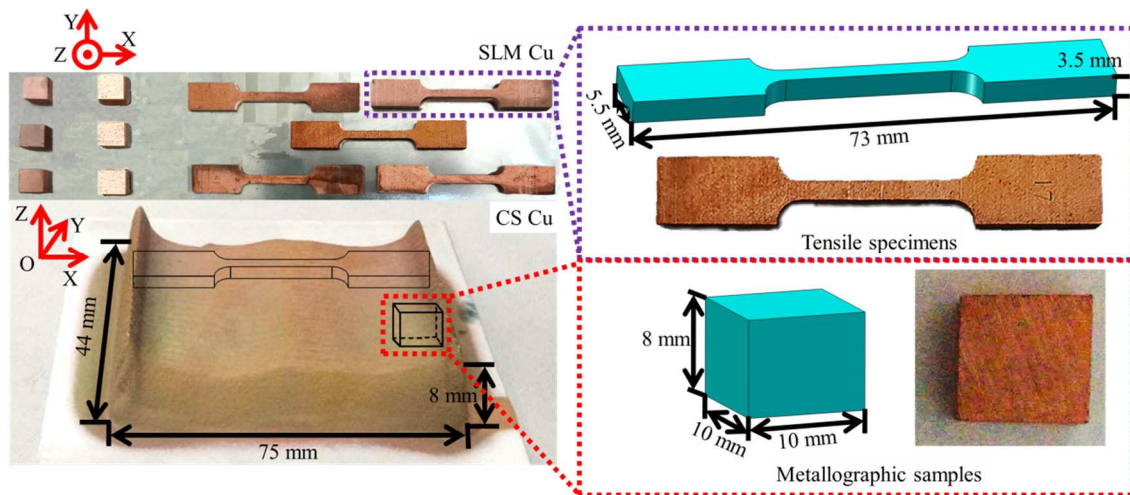
174 The relative density of the SLM Cu and CS Cu samples was measured by an  
 175 analytical balance (ABZ 200C, PCE instruments, Germany) based on Archimedes  
 176 principle using the following Eq. (1):

177 
$$\frac{\rho_A}{\rho_{\text{standard}}} = \frac{\rho_{\text{water}} \cdot m_{A(\text{air})}}{\rho_{\text{standard}} \cdot (m_{A(\text{air})} - m_{A(\text{water})})} \quad (1)$$

178 where  $\rho_A$  is the density of SLM Cu or CS Cu samples;  $\rho_{\text{standard}}$  is the standard  
 179 density of the pure copper part [28];  $m_{A(\text{air})}$  is the average mass of the SLM Cu or CS  
 180 Cu samples in air;  $m_{A(\text{water})}$  is the mean mass value of the SLM Cu or CS Cu  
 181 specimens in water;  $\rho_{(\text{water})}$  is the density of water. Three parts were tested and  
 182 averaged to determine the relative density. All specimens were polished utilizing SiC  
 183 grinding papers with an increasing grits from 400<sup>#</sup> to 4000<sup>#</sup>. Then, all the specimens  
 184 for metallographic analysis were polished using Al<sub>2</sub>O<sub>3</sub> suspensions. After that, each  
 185 sample was etched for 50 s in a homemade solution (2 ml HCl, 1 ml Fe<sub>3</sub>Cl, and 97 ml  
 186 C<sub>2</sub>H<sub>5</sub>OH). The microstructure characteristics were detected via an optical microscope  
 187 (OM, Leica Dmi5000m, Germany) and a scanning electron microscopy (SEM)  
 188 machine (FEI Nova NanoSEM 450, United States). Phase distribution of the SLM Cu  
 189 and CS Cu parts was identified by a X-ray diffraction (XRD, Siemens, Germany)  
 190 equipment in a continuous scanning type at 40 kV and 100 mA in a 2θ range of  
 191 30-100°.

192 **2.3 Physical and mechanical property tests**

193 The electrical conductivity of SLM Cu and CS Cu specimens was measured at  
194 room temperature (around 20 °C) using an eddy conductivity meter (Huatech HEC102,  
195 China) at 60 KHz according to the ASTM E1004-17 standard. Note that the  
196 measuring direction of the electrical conductivity test is in the XY plane, as depicted  
197 in Fig. 2. Three measurements of each specimen should be collected and then  
198 averaged with the corresponding standard deviations determined. These samples were  
199 polished and prepared for microhardness determination. Vickers microhardness  
200 measurements of these parts were investigated using a Leitz-Wetzlar tester with a load  
201 of 50 g for a dwell time of 15 s. For each sample, ten measurements were taken from  
202 random positions on the polished cross-section of the sample in the XY plane (as  
203 shown in Fig. 2) and averaged to obtain a mean value.



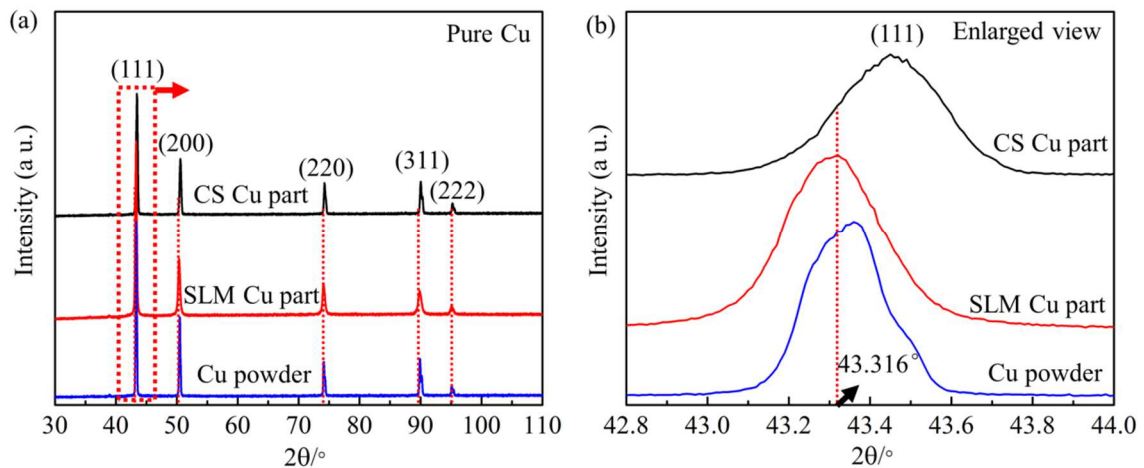
204  
205 **Fig. 2.** Metallographic samples and tensile specimens fabricated using SLM and CS technology.

206 Tensile tests were conducted in ambient temperature (approximately 20 °C) at a  
207 displacement of 10 mm/min in accordance with the ASTM E8M. The static tensile  
208 properties data, including ultimate tensile strength (UTS), yield strength (YS) and  
209 crosshead displacement was measured directly from a tensile machine (INSTRON  
210 5982, USA). The total elongation at break (EL) of these tensile specimens was  
211 measured and calculated with the help of ASTM E111 standard. The tensile strain to  
212 failure was measured employing a strain gauge and an electronic extensometer with a  
213 gauge of 10 mm. Notably, three tensile specimens were considered as a test group,  
214 and the mean value of each group was calculated and recorded. The fracture surfaces  
215 of the tensile parts were detected utilizing SEM to determine the mode of the fracture  
216 and to analyze the mechanism of tensile fracture of SLM Cu parts and CS Cu samples,  
217 respectively.

## 218 3 Results and analysis

### 219 3.1 Phases analysis

220 According to the XRD spectrum of the Cu samples fabricated via SLM or CS  
221 technology, as depicted in Fig. 3a, only peaks related to pure Cu phase was detected.  
222 Besides, it can be further concluded that no obvious oxidation phenomenon occurred  
223 during the manufacture process of CS Cu parts or SLM Cu samples. As detected in  
224 Fig. 3b, the diffraction peaks position and shape of the Cu samples both changed as  
225 compared to the (111) crystal plane of the standard pure Cu phase. Amongst these  
226 samples, the diffraction peak of the SLM Cu sample was shifted to a low-angle  
227 direction, while, the diffraction peak of the CS Cu specimen was shifted to a  
228 high-angle position compared with the standard diffraction peak position of the pure  
229 Cu phase. It is interesting to find that the full width at half maximum (FWHM) of the  
230 Cu powders is narrower than that of the CS Cu and SLM Cu specimens. Additionally,  
231 the lattice constants of the Cu parts fabricated via SLM or CS technology were  
232 calculated using the Rietveld Refinement method [29,30] and are presented in Table 3.  
233 According to Table 3, the measured lattice constants of Cu phase ( $a=3.61857 \text{ \AA}$ ) in the  
234 SLM parts were larger than the standard lattice constant of Cu phase ( $a=3.615 \text{ \AA}$ ).  
235 However, the lattice constant measured in the CS Cu sample ( $a=3.61065 \text{ \AA}$ ) was  
236 lowest among these samples and the Cu powders.



237  
238 **Fig. 3.** (a) XRD profiles of the Cu parts manufactured using different AM techniques; (b) the magnified  
239 view of the (111) crystal plane.

240 Multiple factors such as grain size, surface stress, and etc. will result in changes  
241 in the XRD diffraction peaks and the lattice distortion. As CS Cu specimens are  
242 formed by depositing numerous Cu power particles with large deformation, residual  
243 compressive stress still distributed on the sample surface. Thus, interplanar distance  
244 will become smaller, and the peak of the CS Cu parts will be shifted to a high-angle

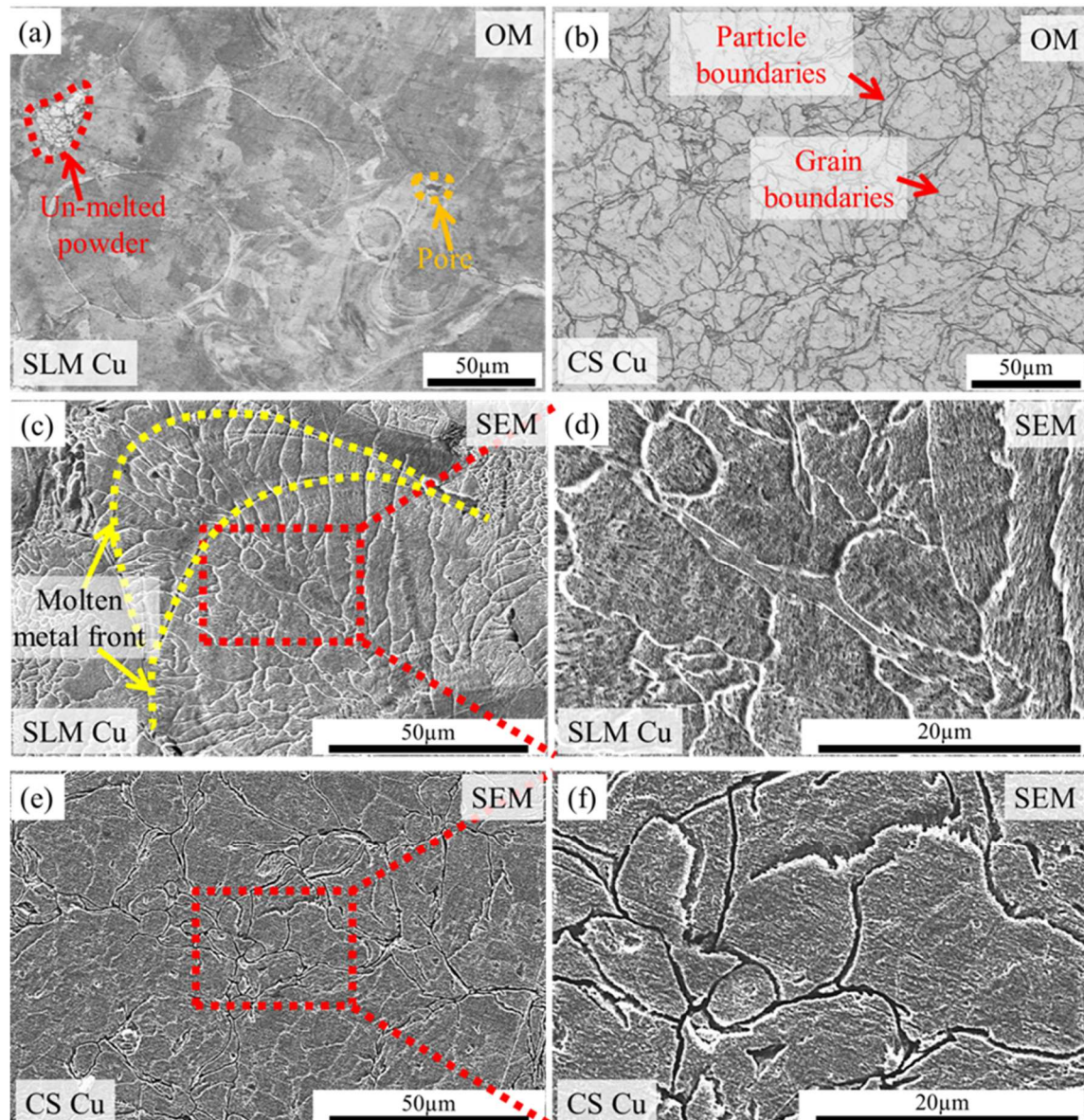
245 position, as shown in Fig. 3b. The lattice constant will smaller than that of standard  
 246 Cu phase, as calculated in Table 3. As for the SLM process, the SLM Cu parts are  
 247 created after experiencing a series of rapid melting and solidifying procedures. The  
 248 residual tensile stress will exit in the SLM Cu samples. Therefore, the interplanar  
 249 distance will grow larger, and the peak position will be shifted to a low-angle  
 250 direction, as depicted in Fig. 3b. Moreover, owing to the rapid solidification process  
 251 will lead to a lattice distortion phenomenon of the generated Cu grains, the lattice  
 252 parameter of the SLM Cu sample is larger than that of the standard Cu phase, as  
 253 described in Table 3. It is worth noting that, regardless of the CS Cu process or SLM  
 254 Cu procedure, the grains formed in these Cu samples are relatively smaller than the  
 255 grain of the Cu powders due to the inherent nature of these AM techniques. Therefore,  
 256 the FWHM of the CS Cu and SLM Cu samples are wider than the FWHM of the Cu  
 257 powders, as detected in Fig. 3b.

258 **Table 3:** Lattice constants of the Cu phase formed in the SLM Cu and CS Cu parts

Samples	Lattice constant (Å)	Fitting error
Standard Cu phase [31]	3.615	/
Cu powders	3.61543	≤10.87
CS Cu parts	3.61065	≤10.12
SLM Cu parts	3.61857	≤10.21

### 259 3.2 Microstructural evolution

260 Fig. 4 displays the XY cross-sectional OM and SEM pictures of the etched Cu  
 261 parts fabricated using SLM or CS technology. In the SLM Cu part as depicted in Fig.  
 262 4a, after experiencing a rapid melting and solidification process, some un-melted  
 263 powder (red arrow) and pore (orange arrow) are still distributed at the solidified  
 264 molten metal interface. Due to the low absorption rate of the long-wavelength laser  
 265 energy by pure Cu powder (approximately 44 % [32]) and the high thermal  
 266 conductivity of solidified pure Cu layers, the solidification speed of the laser molten  
 267 pool is extremely high and further the solidified molten metal interface becomes  
 268 obviously visible, as shown in Fig. 4c. Besides, columnar dendrites with a certain  
 269 growth direction and equiaxed grains can be formed in the solidified molten metal and  
 270 the interface between the adjacent solidified molten metals, respectively, which  
 271 indicate that typical non-equilibrium microstructures can be detected in SLM Cu  
 272 sample as shown in Fig. 4c. It is interesting to find that cellular and columnar  
 273 substructures constitute the polycrystalline grains of the SLM Cu part as revealed in  
 274 Fig. 4d.



275  
 276 **Fig. 4.** XY cross-sectional microstructure of the etched Cu samples processed using different AM  
 277 techniques: (a) microstructure of the SLM Cu sample detected using OM; (b) microstructure of the CS  
 278 Cu sample observed using OM; (c) microstructure of the SLM Cu sample detected using SEM; (d)  
 279 magnified view of c; (e) microstructure of the CS Cu sample observed using SEM; (f) magnified view  
 280 of e.

281 Different with the microstructure of the SLM Cu sample, as detected in Fig. 4b,  
 282 e-f, it is distinct that Cu particles underwent intensely serious plastic deformation after  
 283 CS deposition process. In the CS Cu as-built state as displayed in Fig. 4b, both  
 284 powder particles boundaries and grains boundaries get detectable after etching.  
 285 Notably, the etching is more conspicuous at the powder particles boundaries between  
 286 the neighboring particles than at the grains boundaries of the CS Cu specimen, which  
 287 indicates that the particle boundary is the region most vulnerable to corrosion. In the  
 288 CS Cu deposition process, the high-speed impact brought a large plastic deformation  
 289 to spherical powder particles, resulting in a serious compression and flattening of the

290 Cu powder in the Z direction, as shown in Fig. 2 [33]. Consequently, the particle  
291 contour exhibited an equiaxed shape in the XY cross-section as presented in Fig. 4b, e.  
292 Additionally, as depicted in Fig. 4e, the substructures of the polycrystalline grains  
293 were not detected, which is a different point with the microstructure of the SLM Cu  
294 specimen.

295 Note that the reason for these microstructural differences can be attributed to the  
296 fundamental differences in the material preparation processes of SLM technology and  
297 CS technology. The manufacturing of the SLM Cu samples is a metallurgical process.  
298 Thanks to the high-velocity cooling rate ( $10^6$ - $10^8$  K/s [34]) of the molten pool, fine  
299 microstructure and substructure can be formed during the SLM process. Unlike the  
300 SLM processing, CS technology is a mechanical process in which powder particles  
301 undergo severe plastic deformation and then gradually accumulate into a solid layer.  
302 Since it is difficult for powder particles to produce the metallurgical reactions during  
303 the CS deposition process, the microstructure of the deposited layer is supposed to be  
304 similar to that of powder particles. The commercial pure Cu powders utilized in this  
305 research were manufactured by a gas atomization (GA) process. However, although a  
306 lower cooling rate ( $10^3$ - $10^6$  K/s [35,36]) produced by GA than that of the SLM  
307 process, Cu particles are shattered after repeated impacts, causing the polycrystalline  
308 grains in the powder particles to break into a large number of fine and unevenly  
309 distributed equiaxed grains.

### 310 **3.3 Main properties**

#### 311 **3.3.1 Physical properties**

312 The averaged electrical conductivity of the pure Cu parts via SLM or CS  
313 technology is revealed in Fig. 5. According to the statistical data, the averaged  
314 electrical conductivity of SLM Cu part is only 23.9 MS/m, i.e. about 41 % IACS,  
315 while the mean value of the electrical conductivity of CS Cu part is 42.3 MS/m  
316 (around 73 % IACS). The average electrical conductivity of the CS Cu sample is  
317 approximately 178 % of that of the SLM Cu sample.

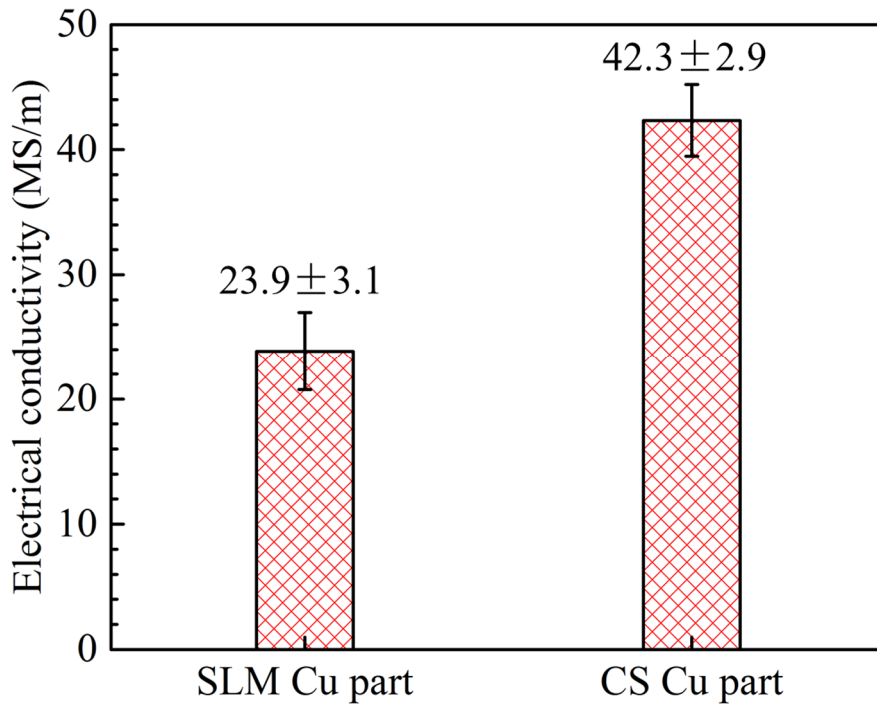


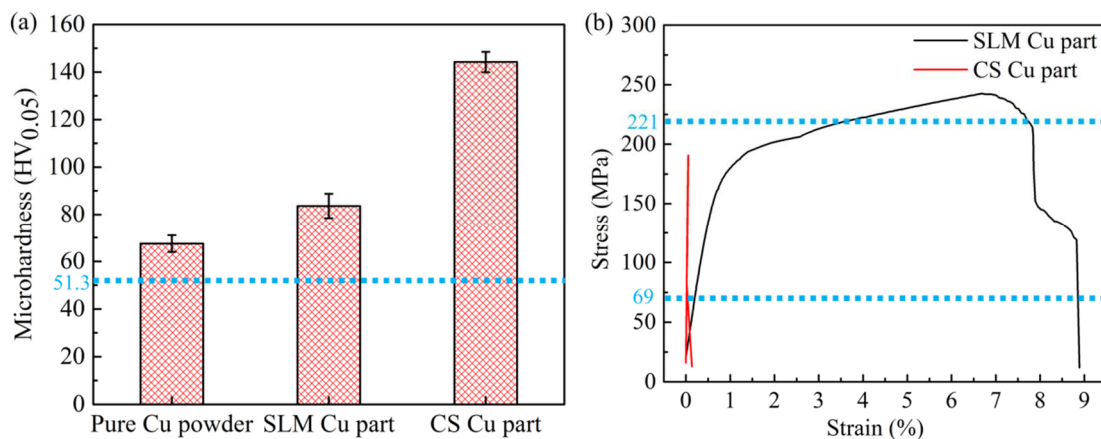
Fig. 5. Averaged electrical conductivity of the SLM Cu part and the CS Cu part

Main factors affecting the conductive properties of the solid pure metals include working temperature, atomic lattice structure, impurities, microstructural defects and anisotropy, etc. Notably, the same raw materials and testing methods were applied using in this study. Thus, the atomic lattice structure, microstructural defects and anisotropy can be considered as the main elements affecting the conductive properties of these Cu samples. As demonstrated in Fig. 4a-f and analysis mentioned above, not only a large number of columnar dendrites with a certain growth direction, equiaxed crystals, and substructures were produced in the SLM Cu sample, but also a prominent microstructural anisotropy phenomenon. In addition, due to the poor weldability of Cu powder, un-melted powder and pores can also cause an increased microstructural defect phenomenon in the SLM Cu part. However, compared to the SLM Cu sample, CS Cu specimen is equivalent to a metal part produced by the cold working process with a large plastic deformation. Although, the microstructural defects including dislocations, vacancies and voids arise by the CS Cu deposition process, these defects contribution to the electrical conductivity is negligibly small at room temperature [37]. Besides, the density measurement showed that the relative density of the SLM Cu and the CS Cu sample was  $98.8 \pm 0.5 \%$  and  $99.2 \pm 0.4 \%$ , respectively. Thus, it can be considered that the defect is not the main factor affecting the electrical conductivity of these additive manufactured samples in this study. Additionally, the CS Cu deposition process lead to achieve isotropic microstructure i.e. equiaxed grains, and less substructures formed in these grains. As such, in the as-built state, the electrical conductivity of the CS Cu part is better than that of the SLM Cu

342 part.

### 343 3.3.2 Hardness and tensile properties

344 Mechanical properties of the pure Cu parts processed via SLM or CS technology  
345 including microhardness and the stress-strain curves are presented in Fig. 6. The  
346 statistical data of the corresponding mechanical properties are shown in Table 4.  
347 Amongst these specimens, the mean microhardness of the CS Cu samples is the  
348 highest, which is about 172 % of that of SLM Cu parts and around 214 % of that of  
349 pure Cu powders. Moreover, because of the similar nominal chemical composition  
350 between the feedstock powders utilized in this study and the wrought C11000 Cu  
351 component, the wrought C11000 Cu part is regarded as the reference for comparison.  
352 The average microhardness of the SLM copper samples is 64 % higher than the  
353 minimal microhardness of the wrought C11000 copper. It can be interesting found that  
354 the microhardness of both Cu powders and Cu samples processed using SLM or CS  
355 technology is higher than that of the minimal threshold of the C11000 Cu parts. Note  
356 that the reasons for the difference in the average microhardness of the Cu samples can  
357 be attributed to the surface residual stress and the microstructure generated in the Cu  
358 specimens. As for the CS Cu deposition process, the compressive residual stress is  
359 principally distributed on the surface of the CS Cu part [38], while, the tensile residual  
360 stress is mainly distributed on the surface of the SLM Cu sample after SLM  
361 processing [39,40]. Therefore, the averaged microhardness of the CS Cu parts is  
362 higher than others. Moreover, compared with the microstructure of the wrought  
363 C11000 Cu component [28], both the microstructure of the raw materials applied in  
364 this study and the Cu samples produced using SLM or CS technology is finer than  
365 that of the wrought C11000 Cu component. Consequently, the microhardness of these  
366 samples is higher than that of the minimal threshold of the wrought C11000 Cu part.



367

368 **Fig. 6.** Mechanical properties of the pure Cu parts processed via SLM or CS technology: (a)

369

microhardness; (b) stress-strain curves

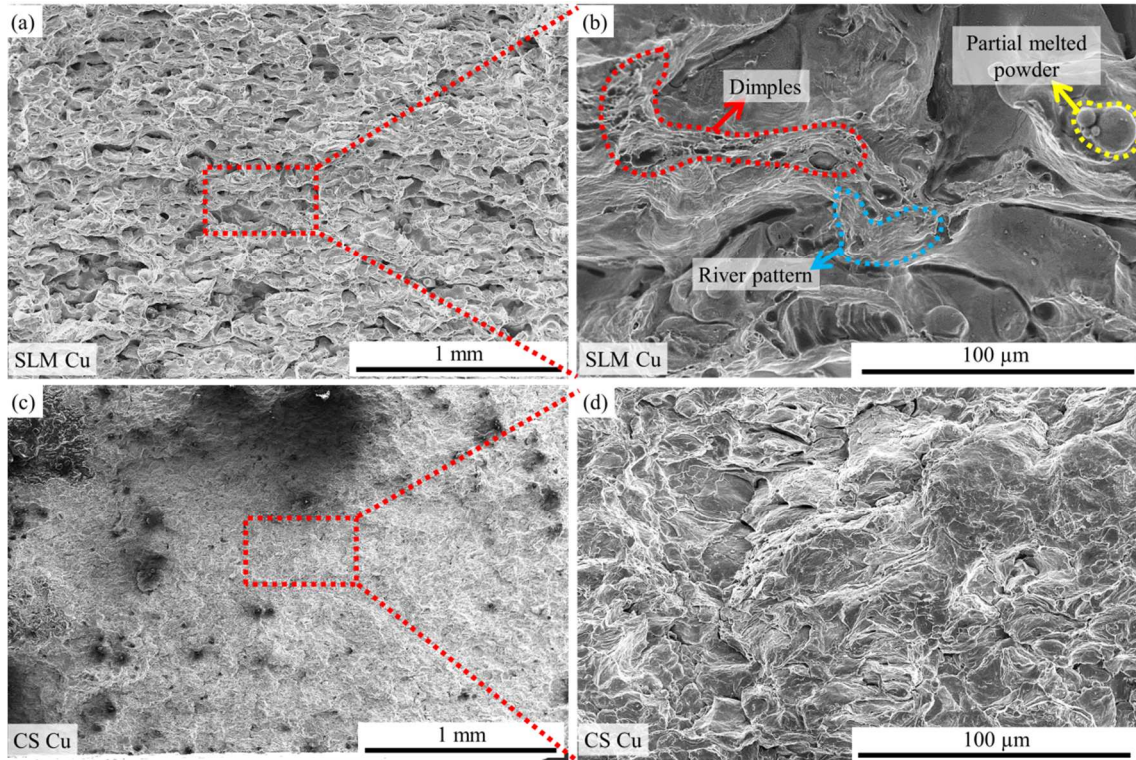
370 The mechanical interlocking phenomenon existed between the Cu powder  
 371 particles results in poor tensile properties of the CS Cu parts, as displayed in Fig. 6  
 372 and Table 4. The UTS of the CS Cu samples is even lower than the minimum UTS of  
 373 the wrought C11000 Cu sample. Additionally, due to a relatively good metallurgical  
 374 bonding condition presented in the SLM Cu part, the SLM Cu specimen exhibits  
 375 excellent tensile properties, e.g., the YS and UTS of the SLM Cu part is  
 376 approximately 177 % and 110 % of the minimum YS and UTS of the wrought  
 377 C11000 Cu part, respectively. Note that the stress-strain curve shows that the CS Cu  
 378 samples are very brittle and the premature fracture is due to the brittleness of the  
 379 material after hardening, which is induced by the severe plastic deformation at high  
 380 strain rate during the impact, not strictly to the mechanical interlocking. That is to say  
 381 that we can have the same behavior even if the fracture failure is not directly related  
 382 to mechanical interlocking. The comparison clearly demonstrated that the SLM Cu  
 383 samples fabricated in this work can meet the minimum requirement of wrought parts.

384 **Table 4:** Mechanical properties of the pure Cu samples manufactured using different AM techniques  
 385 and the reference materials

Samples	Microhardness (HV <sub>0.05</sub> )	YS (MPa)	UTS (MPa)	EL (%)
Pure Cu powder	67.5±3.5	/	/	/
SLM Cu part	83.6±5.2	185.8±6.1	242.2±8.2	8.9±2.3
CS Cu part	144.2±4.3	/	191.3±5.2	0.8±0.2
C11000 [28]	51.3-104	69-365	221-455	4-55

### 386 3.3.3 Fracture morphology analysis

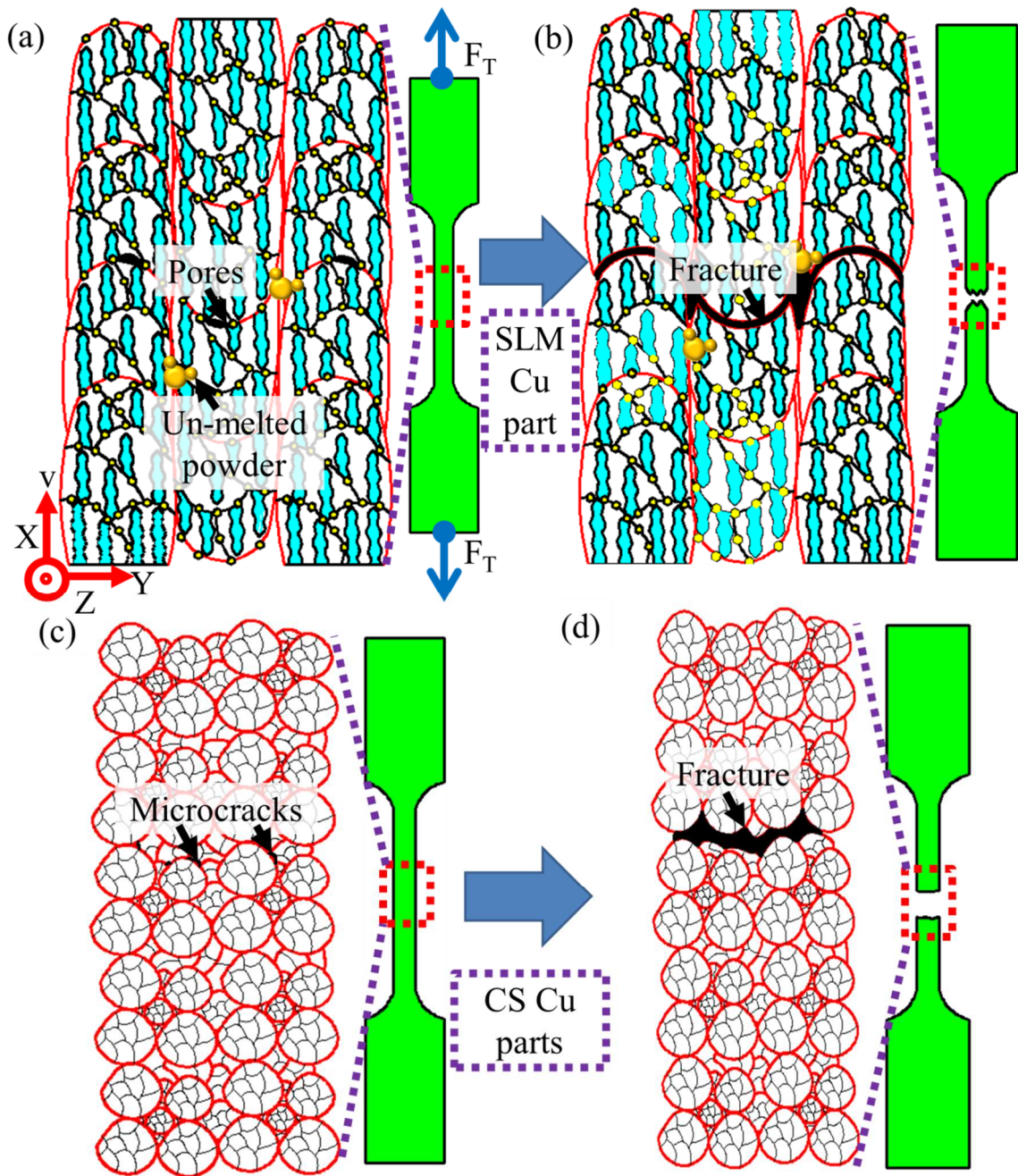
387 For further comparison, the fractographic photos of the tensile samples via SLM  
 388 or CS technology are depicted in Fig. 7. For the SLM Cu samples, as detected in Fig.  
 389 7a-b, the fracture surfaces were observed by both river pattern (blue arrow) and  
 390 dimples (red arrow), which demonstrates that occurrence of both brittle fracture and  
 391 ductile fracture features. With regard to the CS Cu samples, however, the fracture  
 392 morphology revealed only cleavage-like features as shown in Fig. 7c-d, indicating the  
 393 occurrence of inter-particle failure which is an evident index of only brittle fracture  
 394 existing [26]. Note that ductile trans-granular failure is a proof of excellent cohesive  
 395 strength and high ductility [41]. Thus, the fractographic photos illustrate why the UTS  
 396 and EL of the CS Cu parts are not as good as SLM Cu specimens.



397

398 **Fig. 7.** Fracture morphology of the pure Cu parts processed via SLM or CS technology detected using  
 399 SEM: (a) SLM Cu sample; (b) enlarged view of a; (c) CS Cu sample; (d) enlarged view of c.

400 To further illustrate the tensile behavior of the Cu parts manufactured via  
 401 different AM techniques, the schematic of relationship between microstructure and  
 402 tensile behavior can be presented in Fig. 8. For the SLM Cu part, due to the  
 403 distinctive features of the pure Cu powders, e.g., low laser absorption rate and  
 404 excellent thermal conductivity, the solidification rate of the molten copper metal is  
 405 extremely high. Hence, these characteristics result in a poor fusion condition between  
 406 adjacent laser tracks. As depicted in Fig. 8a, microstructural defects such as un-melted  
 407 powders and pores are still existed in the interface of the neighboring laser tracks.  
 408 During the tensile test process, the fracture phenomenon easily happens at the  
 409 solidified molten metal interface in the SLM Cu sample, especially the positions with  
 410 pores and un-melted powders distributed, as revealed in Fig. 8b. Owing to the  
 411 relatively good toughness of the SLM Cu sample, during the testing process, adjacent  
 412 laser tracks will be stretched and then fractured along the interface of the solidified  
 413 molten metal. Thus, the fracture morphology after tensile test exhibits “honeycomb”  
 414 shape, as shown in Fig. 7a. For the CS Cu sample, however, due to the absence of the  
 415 metallurgical phenomenon during the CS Cu process, the mechanical interlocking  
 416 method is a main bonding manner among these Cu powders. As such, during the  
 417 tensile test, a large number of microcracks are produced and propagated at the  
 418 interface of the Cu particles and till large fractures are formed, as demonstrated in Fig.  
 419 8b.



420  
421  
422  
423

Fig. 8. Microstructure features of the Cu parts manufactured via different AM techniques in the tensile test: (a) SLM Cu sample before tensile test; (b) SLM Cu sample after tensile test; (c) SLM CS Cu specimen before tensile test; (d) CS Cu specimen after tensile test.

424  
425  
426  
427  
428  
429  
430  
431

Although CS Cu parts have good electrical conductivity, the challenging problems such as insufficient bonding strength and low manufacturing accuracy are still great challenging in the field of CS technology. However, due to the low laser absorption rate of the pure Cu powders, the inherent defects and microstructural anisotropy of the SLM Cu parts still lead to a poor physical property like electrical conductivity compared to the CS Cu components. As such, in the future research, it is necessary to carry out more experiments and mechanism analysis based on the above problems to manufacture better Cu components with excellent microstructure and

432 comprehensive properties.

## 433 **4 Conclusions**

434 In summary, cold spray technology and selective laser melting technology is the  
435 promising metal additive manufacturing techniques. For evaluating and comparing of  
436 the main properties of SLM Cu and CS Cu parts, the microstructure features, physical  
437 and mechanical properties, and tensile behavior of Cu parts fabricated via SLM and  
438 CS technologies are studied in detail. The following are the primary conclusions  
439 derived from the current work were listed as follows:

440 1. The XRD spectrum revealed that only Cu phase is formed in the SLM Cu  
441 parts and CS Cu samples. The lattice constant of the Cu phase in the CS Cu part  
442 ( $a=3.61065 \text{ \AA}$ ) was the lowest among these samples, due to the residual compressive  
443 stress. However, the lattice parameter of the Cu phase in the SLM Cu sample  
444 ( $a=3.61857 \text{ \AA}$ ) was the largest amongst these parts owing to a lattice distortion  
445 phenomenon of the produced Cu grains.

446 2. The microstructure of the SLM Cu parts presented the polycrystalline grains  
447 with substructures including the columnar dendrites and the equiaxed structures. As  
448 for the CS Cu samples, only the equiaxed grains were detected. The substructures,  
449 however, cannot be found in the CS Cu specimens.

450 3. The averaged electrical conductivity of SLM Cu part is only 23.9 MS/m  
451 (about 41 % IACS), while the mean value of the electrical conductivity of CS Cu part  
452 is 42.3 MS/m (around 73 % IACS). In terms of the microhardness, the average  
453 microhardness value of the CS Cu samples is 172 % of that of SLM Cu samples. With  
454 regard to the tensile properties, the YS and UTS of the SLM Cu specimens is  
455 approximately 177 % and 110 % of the minimum YS and UTS of the wrought  
456 C11000 Cu part, respectively.

457 The present investigation demonstrates that the different metal AM technologies  
458 have distinguished influence on the microstructure, phase distribution, static  
459 properties of the Cu parts via SLM or CS technology. This study will attract the great  
460 attention of the engineering community for selecting a proper AM technology to  
461 obtain a desirable Cu component with excellent microstructure and comprehensive  
462 performances. Now, the focus of this article is to preliminary study the comparison of  
463 the microstructure and main properties of copper samples manufactured utilizing the  
464 two types of AM technologies. Based on this, studies about the effect of heat  
465 treatments on the microstructure and properties of the SLM and CS Cu samples are  
466 our next research point.

## 467 **Acknowledgement**

468 This work is supported by Sciences Platform Environment and Capacity Building  
469 Projects of GDAS (2019GDASYL-0402004, 2019GDASYL-0502006,  
470 2020GDASYL-20200103108, 2019GDASYL-0402006, 2020GDASYL-20200402005,  
471 2018GDASCX-0402, 2018GDASCX-0111 and 2019GDASYL-0501009), Guangzhou Project  
472 of Science & Technology (201909010008, 201807010030), Guangdong province Science and  
473 Technology Plan Projects (2019A1515011841, 2017A070701027, 2017A070702016,  
474 2014B070705007 and 2017B030314122). Yunnan Science and Technology Talent and  
475 Platform Program (Academician Expert Workstation) No. 2018IC080, International  
476 Cooperation Project (Grants No. 201807010013). Cheng Chang would like to thank the  
477 support from the program of CSC (201801810106).

## 478 **References**

- 479 [1] G. Ian, D.W. Rosen, B. Stucker, Additive Manufacturing Technologies-Rapid Prototyping to  
480 Direct Digital Manufacturing, Springer Science & Business Media, New York, 2010.  
481 doi:10.1007/978-3-662-53120-4\_16866.
- 482 [2] F. Singer, D.C. Deisenroth, D.M. Hymas, M.M. Ohadi, Additively manufactured copper  
483 components and composite structures for thermal management applications, Proc. 16th Intersoc.  
484 Conf. Therm. Thermomechanical Phenom. Electron. Syst. ITherm 2017. (2017) 174–183.  
485 doi:10.1109/ITHERM.2017.7992469.
- 486 [3] W. Li, K. Yang, S. Yin, X. Yang, Y. Xu, R. Lupoi, Solid-state additive manufacturing and  
487 repairing by cold spraying: A review, J. Mater. Sci. Technol. 34 (2018) 440–457.  
488 doi:10.1016/j.jmst.2017.09.015.
- 489 [4] X. Yan, C. Chen, C. Chang, D. Dong, R. Zhao, R. Jenkins, J. Wang, Z. Ren, M. Liu, H. Liao, R.  
490 Lupoi, Study of the microstructure and mechanical performance of C-X stainless steel  
491 processed by selective laser melting ( SLM ), Mater. Sci. Eng. A. 781 (2020) 139227.  
492 doi:10.1016/j.msea.2020.139227.
- 493 [5] S. Yin, Y. Xie, J. Cizek, E.J. Ekoi, T. Hussain, D.P. Dowling, R. Lupoi, Advanced  
494 diamond-reinforced metal matrix composites via cold spray: Properties and deposition  
495 mechanism, Compos. Part B Eng. 113 (2017) 44–54. doi:10.1016/j.compositesb.2017.01.009.
- 496 [6] S. Yin, J. Cizek, C. Chen, R. Jenkins, G. O'Donnell, R. Lupoi, Metallurgical bonding between  
497 metal matrix and core-shelled reinforcements in cold sprayed composite coating, Scr. Mater.  
498 177 (2020) 49–53. doi:10.1016/j.scriptamat.2019.09.023.
- 499 [7] X. Yan, S. Yin, C. Chen, R. Jenkins, R. Lupoi, R. Bolot, W. Ma, M. Kuang, H. Liao, J. Lu, M.  
500 Liu, Fatigue strength improvement of selective laser melted Ti6Al4V using ultrasonic surface  
501 mechanical attrition, Mater. Res. Lett. 7 (2019) 327–333.  
502 doi:10.1080/21663831.2019.1609110.
- 503 [8] C. Chang, X. Yan, R. Bolot, J. Gardan, S. Gao, Influence of post-heat treatments on the  
504 mechanical properties of CX stainless steel fabricated by selective laser melting, J. Mater. Sci.

- 505 (2020) 1–14. doi:10.1007/s10853-020-04566-x.
- 506 [9] X. Yan, Q. Li, S. Yin, Z. Chen, R. Jenkins, C. Chen, J. Wang, W. Ma, R. Bolot, R. Lupoi, Z.  
507 Ren, H. Liao, M. Liu, Mechanical and in vitro study of an isotropic Ti6Al4V lattice structure  
508 fabricated using selective laser melting, *J. Alloys Compd.* 782 (2019) 209–223.  
509 doi:10.1016/j.jallcom.2018.12.220.
- 510 [10] S. Saedi, S.E. Saghaian, A. Jahadakbar, N. Shayesteh Moghaddam, M. Taheri Andani, S.M.  
511 Saghaian, Y.C. Lu, M. Elahinia, H.E. Karaca, Shape memory response of porous NiTi shape  
512 memory alloys fabricated by selective laser melting, *J. Mater. Sci. Mater. Med.* 29 (2018).  
513 doi:10.1007/s10856-018-6044-6.
- 514 [11] X. Yan, C. Chen, R. Zhao, W. Ma, R. Bolot, J. Wang, Z. Ren, H. Liao, M. Liu, Selective laser  
515 melting of WC reinforced maraging steel 300: Microstructure characterization and tribological  
516 performance, *Surf. Coatings Technol.* 371 (2018) 355–365.  
517 doi:10.1016/j.surfcoat.2018.11.033.
- 518 [12] S. Yin, W. Li, B. Song, X. Yan, M. Kuang, Y. Xu, K. Wen, R. Lupoi, Deposition of  
519 FeCoNiCrMn high entropy alloy (HEA) coating via cold spraying, *J. Mater. Sci. Technol.* 35  
520 (2019) 1003–1007. doi:10.1016/j.jmst.2018.12.015.
- 521 [13] S. Yin, P. Cavaliere, B. Aldwell, R. Jenkins, H. Liao, W. Li, R. Lupoi, Cold spray additive  
522 manufacturing and repair: Fundamentals and applications, *Addit. Manuf.* 21 (2018) 628–650.  
523 doi:10.1016/j.addma.2018.04.017.
- 524 [14] C. Chen, Y. Xie, X. Xie, X. Yan, R. Huang, J. Wang, Z. Ren, S. Deng, H. Liao, Effects of  
525 substrate heat accumulation on the cold sprayed Ni coating quality: Microstructure evolution  
526 and tribological performance, *Surf. Coatings Technol.* 371 (2019) 185–193.  
527 doi:10.1016/j.surfcoat.2019.04.090.
- 528 [15] C. Chen, Y. Xie, X. Yan, R. Huang, M. Kuang, W. Ma, R. Zhao, J. Wang, M. Liu, Z. Ren, H.  
529 Liao, Cold sprayed WC reinforced maraging steel 300 composites: Microstructure  
530 characterization and mechanical properties, *J. Alloys Compd.* 785 (2019) 499–511.  
531 doi:10.1016/j.jallcom.2019.01.135.
- 532 [16] P. Anatolii, K. Vladimir, S. Klinkov, A. Alkimov, V. Fomin, *Cold Spray Technology*, Elsevier,  
533 2006.
- 534 [17] Q. Wang, K. Spencer, N. Birbilis, M.X. Zhang, The influence of ceramic particles on bond  
535 strength of cold spray composite coatings on AZ91 alloy substrate, *Surf. Coatings Technol.* 205  
536 (2010) 50–56. doi:10.1016/j.surfcoat.2010.06.008.
- 537 [18] S. Yin, X. Wang, X. Suo, H. Liao, Z. Guo, W. Li, C. Coddet, Deposition behavior of thermally  
538 softened copper particles in cold spraying, *Acta Mater.* 61 (2013) 5105–5118.  
539 doi:10.1016/j.actamat.2013.04.041.
- 540 [19] C. Chen, Y. Xie, X. Yan, S. Yin, H. Fukunuma, R. Huang, R. Zhao, J. Wang, Z. Ren, M. Liu,  
541 H. Liao, Effect of hot isostatic pressing (HIP) on microstructure and mechanical properties of  
542 Ti6Al4V alloy fabricated by cold spray additive manufacturing, *Addit. Manuf.* 27 (2019) 595–  
543 605. doi:10.1016/j.addma.2019.03.028.
- 544 [20] S. Bagherifard, A. Heydari Astaraee, M. Locati, A. Nawaz, S. Monti, J. Kondás, R. Singh, M.  
545 Guagliano, Design and analysis of additive manufactured bimodal structures obtained by cold  
546 spray deposition, *Addit. Manuf.* 33 (2020) 101131. doi:10.1016/j.addma.2020.101131.
- 547 [21] Copper as electrical conductive material with above-standard performance properties, (2015)  
548 1–38. <http://www.conductivity-app.org/single-article/cu-overview#L15>.

- 549 [22] Y.S. Zhang, Z. Han, K. Lu, Fretting wear behavior of nanocrystalline surface layer of copper  
550 under dry condition, *Wear*. 265 (2008) 396–401. doi:10.1016/j.wear.2007.11.004.
- 551 [23] P.X. Jiang, M.H. Fan, G.S. Si, Z.P. Ren, Thermal-hydraulic performance of small scale  
552 micro-channel and porous-media heat-exchangers, *Int. J. Heat Mass Transf.* 44 (2001) 1039–  
553 1051. doi:10.1016/S0017-9310(00)00169-1.
- 554 [24] ASM handbook, volume 2, Properties and Selection: Nonferrous Alloys and Special-Purpose  
555 Materials, 1990. doi:10.1007/s004310050884.
- 556 [25] C. Silbernagel, L. Gargalis, I. Ashcroft, R. Hague, M. Galea, P. Dickens, Electrical resistivity  
557 of pure copper processed by medium-powered laser powder bed fusion additive manufacturing  
558 for use in electromagnetic applications, *Addit. Manuf.* 29 (2019) 100831.  
559 doi:10.1016/j.addma.2019.100831.
- 560 [26] S. Yin, R. Jenkins, X. Yan, R. Lupoi, Microstructure and mechanical anisotropy of additively  
561 manufactured cold spray copper deposits, *Mater. Sci. Eng. A*. 734 (2018) 67–76.  
562 doi:10.1016/j.msea.2018.07.096.
- 563 [27] W.Y. Li, S. Yin, X.F. Wang, Numerical investigations of the effect of oblique impact on  
564 particle deformation in cold spraying by the SPH method, *Appl. Surf. Sci.* 256 (2010) 3725–  
565 3734. doi:10.1016/j.apsusc.2010.01.014.
- 566 [28] ASM International Handbook Committee, ASM Speciality Handbook, Copper and Copper  
567 Alloys, 2001.
- 568 [29] L. Alexander, H.P. Klue, Basic aspects of x-ray absorption in quantitative diffraction analysis  
569 of powder mixtures, *Powder Diffr.* 4 (1989) 66–69. doi:10.1017/S0885715600016432.
- 570 [30] Materials Information Company, ASM International Handbook Committee, Properties and  
571 selection: irons steels and high performance alloys, *ASM Handb.* (1991) 1872–1873.  
572 doi:10.31399/asm.hb.v01.a0001046.
- 573 [31] S. Graulis, D. Chateigner, R.T. Downs, A.F.T. Yokochi, M. Quirós, L. Lutterotti, E. Manakova,  
574 J. Butkus, P. Moeck, A. Le Bail, Crystallography Open Database - An open-access collection  
575 of crystal structures, *J. Appl. Crystallogr.* 42 (2009) 726–729.  
576 doi:10.1107/S0021889809016690.
- 577 [32] Y. Shenping, Z. Anfeng, L. Shaoduan, W. Tan, Measurement of Laser Light Absorptivity of  
578 Commonly Used Metals in Laser Additive Manufacturing Technique, *Aeronaut. Manuf.*  
579 *Technol.* (2017) 97–100. doi:10.16080/j.issn1671-833x.2017.17.097.
- 580 [33] H. Assadi, H. Kreye, F. Gärtner, T. Klassen, Cold spraying – A materials perspective, *Acta*  
581 *Mater.* 116 (2016) 382–407. doi:10.1016/j.actamat.2016.06.034.
- 582 [34] A.H. Maamoun, Y.F. Xue, M.A. Elbestawi, S.C. Veldhuis, The effect of selective laser melting  
583 process parameters on the microstructure and mechanical properties of Al6061 and AlSi10Mg  
584 alloys, *Materials (Basel)*. 12 (2018). doi:10.3390/ma12010012.
- 585 [35] Z. Fuqian, X. Ming, L. Jianliang, L. Xianyong, G. Weiming, S. An, D. Zhongmin, Study of  
586 rapidly solidified atomization technique and production of metal alloy powders, *Mater. Sci.*  
587 *Eng. A*. 304 (2001) 579–582. doi:10.1016/S0921-5093(00)01538-0.
- 588 [36] C. Si, X. Tang, X. Zhang, J. Wang, W. Wu, Characteristics of 7055Al alloy powders  
589 manufactured by gas-solid two-phase atomization: A comparison with gas atomization process,  
590 *Mater. Des.* 118 (2017) 66–74. doi:10.1016/j.matdes.2017.01.028.
- 591 [37] G. Dyos, *The Handbook of Electrical Resistivity* The Handbook of Electrical Resistivity, 2012.
- 592 [38] V. Luzin, K. Spencer, M.X. Zhang, Residual stress and thermo-mechanical properties of cold

- 593 spray metal coatings, *Acta Mater.* 59 (2011) 1259–1270. doi:10.1016/j.actamat.2010.10.058.
- 594 [39] P. Mercelis, J.P. Kruth, Residual stresses in selective laser sintering and selective laser melting,  
595 *Rapid Prototyp. J.* 12 (2006) 254–265. doi:10.1108/13552540610707013.
- 596 [40] M. Shiomi, K. Osakada, K. Nakamura, T. Yamashita, F. Abe, Residual stress within metallic  
597 model made by selective laser melting process, *CIRP Ann. - Manuf. Technol.* 53 (2004) 195–  
598 198. doi:10.1016/S0007-8506(07)60677-5.
- 599 [41] F. Gärtner, T. Stoltenhoff, J. Voyer, H. Kreye, S. Riekehr, M. Koçak, Mechanical properties of  
600 cold-sprayed and thermally sprayed copper coatings, *Surf. Coatings Technol.* 200 (2006) 6770–  
601 6782. doi:10.1016/j.surfcoat.2005.10.007.
- 602

# Cu samples manufactured via different metal AM techniques

## Microstructural evolution

## Static properties

